Constraining Model Transient Climate Response Using Independent Observations of Solar-Cycle Forcing and Response

By Ka Kit Tung[1], Jiansong Zhou[1] and Charles D. Camp[1,2]

[1]Department of Applied Mathematics, University of Washington, Seattle, Washington, USA. [2]Now at: Department of Mathematics, California Polytechnic State University, San Luis Obispo, California, USA.

ABSTRACT

The coupled atmosphere-ocean models participating in the 4th Assessment Report (AR4) of the Intergovernmental Panel on Climate Change (IPCC) span a large range in their transient climate response (TCR). Using observational results on the response to the 11-year solar variation, we derive a constraint for the TCR. We use five global datasets of long duration, including reanalysis datasets (NCEP/NCAR and ERA-40) and blended *in situ* land-ocean data (GISS, HadCRUT3 and NCDC), and discuss the impact of missing coverage in the *in situ* datasets on our conclusion. It is seen that, compared with our derived constraint, most models assessed by IPCC AR4 have too low a TCR, although their equilibrium climate sensitivity, calculated using a slab ocean model, is close to our lower bound. It appears that in the transient experiments these models may have too high an ocean heat uptake. As a consequence the current models may likely under-predict the transient global warming from increasing greenhouse gases.

1. Introduction.

Transient Climate Response (TCR) is defined in IPCC 4th Assessment Report (AR4) as the global mean warming in response to 1% per year compound increase in CO_2 at the time of its doubling. TCR is deemed more relevant in calibrating models on their ability of predicting the warming resulting from transient increases in CO_2 than the equilibrium climate sensitivity (ECS), which is defined as the equilibrium global mean surface change at doubled CO_2. The coupled atmosphere-ocean models participating in AR4 produce a range of TCR from 1.2 to 2.6 K [*Randall, et al.*, 2007]. This rather large range is difficult to constrain with independent observations, since transient response does not easily discriminate between models with different climate feedback processes [*Hansen, et al.*, 1985]. *Stott et al.* [2006] used the observed 20th century temperature change to constrain three models (HadCM3, GFDL-R30 and PCM) and then applied these models to the calculation of TCR for the future. The calculated TCR is around 2.1 K and the calculated 5-95% probability range is 1.5 to 2.8 K. The rather large range is a result of combining the probability density functions of the three models, which included a model (NCAR's PCM) that is known to have a low climate sensitivity compared to other models. In this work, we propose that the temperature response at the earth's surface to the 11-year solar-cycle variation in total solar irradiance (TSI) can yield a useful constraint on the transient climate response.

2. Datasets and methods.

The solar cycle temperature signal near the surface stands out among larger unforced variability in our climate because its globally coherent spatial structure is mostly one signed (warming) in the zonal mean. The coupled atmosphere-ocean system naturally produces decadal variability of larger amplitude, but this unforced variability often takes the latitude-compensating form of annular modes of warming and cooling [*Marshall, et al.*, 2007] and so can be filtered out using a spatial filter or a simple global average. El Nino-Southern Oscillation (ENSO), although an internal mode of oscillation in the atmosphere-equatorial ocean system, appears to the atmosphere as an "externally forced" response, in the sense that the temperature changes even when globally averaged. Nevertheless, the ENSO spatial pattern is different from the solar response, with warming in the tropics and cooling in the mid-latitudes [*Seager, et al.*, 2003]. (The removal of volcanic-aerosol- induced cooling and the secular trend of global warming, in addition, has been discussed previously [*Camp and Tung*, 2007; *Tung and Camp*, 2008].) To extract the solar cycle response signal by taking advantage of its spatial signature, it is preferable that the dataset we use be globally complete. This was the reason that in our previous work the geographically complete reanalyzed datasets of NCEP/NCAR and ERA-40 were used [*Camp and Tung*, 2007; *Tung and Camp*, 2008]. Both reanalysis data use available station measurements, plus satellite, buoy and other forms of data. These are assimilated by a model, which dynamically supplies the missing information for one variable from constraints provided by other variables. In NCEP/NCAR [*Kalnay, et al.*, 1996], the surface air temperature is derived from observations of upper air variables and surface pressure. In ERA-40 [*Uppala, et al.*, 2005], the surface temperature is called the 2-m temperature. It is not obtained directly as part of the three-dimensional variational analysis of atmospheric fields, but is an interpolation from the lowest model level (at ~10-m) and the background forecast of the skin temperature. Without supplementation by satellite or other data, datasets using *in situ* station measurements of surface temperature have large areas with missing or sparse coverage; these include the Antarctic and the Artic, central African continent, central South America continent, and the northern Asian continent. Interpolation in time and in space tends to reduce the amplitude of the response, which depends on the difference in the anomaly between the solar-max years and the solar-min years.

The land component of the Goddard Institute for Space Studies (GISS) global surface temperature dataset [*Hansen, et al.*, 1999] consists of the monthly mean station data of the Global Historical Climatological Network (GHCN) version 2 of [*Peterson and Vose*, 1997] and the Scientific Committee on Antarctic Research (SCAR) data from Antarctic stations. All station records within 1200 km of a grid point are averaged. In data-sparse regions a single station is used to fill in the estimated temperature up to 1200 km. The ocean component uses the sea-surface temperature (SST) [*Reynolds and Smith*, 1994] rather than the marine air temperature (MAT) because of historical measurement non-uniformity (with respect to ship height and speeds) associated with the latter. From 1982 on, satellite measurements of SST are used, calibrated with the help of thousands of ship and buoy measurements. The same satellite-derived empirical orthogonal functions (EOF) were applied to the period prior to satellite observation [*Smith, et al.*, 1996]. Ship measurements were fitted into these predefined EOFs, which were then used to extend to regions without ship measurements. The Reynolds and Smith SST data are not defined south of 45° S, where available meteorological station measurements over land/islands were used to extend into the ocean area.

HadCRUT3 [*Brohan, et al.*, 2006] is the latest version of the historical blended air surface temperature over land and SST over ocean. The SST in HadSST2 [*Rayner, et al.*, 2006] consists of gridded dataset from *in situ* ship and buoy observations from the new International Comprehensive Ocean-Atmosphere dataset (ICOADS). Over 4000 land stations are used, with additional monthly data obtained from stations in Antarctica. Infilling of missing grid box values using data from surrounding grid boxes, used in the previous versions, is no longer done. Consequently coverage is sparsest over the interior of the continents of Africa and South America, and over Antarctica.

National Climate Data Center (NCDC)'s global merged land-air and SST surface temperature reconstruction [*Smith and Reynolds*, 2005] uses GHCN station data of [*Peterson and Vose*, 1997] and SST data from ICOADS. Approximately 60% of the land surface is sampled, and missing data are filled in using covariance modes but the anomalies are damped to zero in data-sparse areas.

The annual average used here (see legend of Figure 1) starts in December and is slightly different from the calendar year average we used previously. This accounts for the slight difference in the results, of about 0.01K. The period considered is from 1959-2004 for NCEP, GISS, HadCRUT3 and NCDC. ERA-40 is available only up to 2002.

3. Results

Figure 1 shows the 2D composite mean difference (CMD) of the surface temperature of the solar max years and the solar min years for each of the five datasets. Missing data areas are left blank. This figure serves to show that *in situ* dataset such as HadCRUT3 is missing data over large areas in the continents. This situation has not improved in recent decades. It also shows the effect of different interpolation schemes used in filling in the missing data in GISS and NCDC. Figure 2 shows the CMD zonal mean latitudinal patterns. The zonal mean is taken provided that data are available for 2/3 of the longitudes. Otherwise it is left blank. Thus, there is no useful zonal mean information south of 45° S in any of the *in situ* datasets. It is seen in Figures 1 and 2 that the spatial features revealed by all five datasets are very similar. Not surprisingly, the *in situ* datasets with their many regions with missing data requiring interpolation show smaller anomalies than the reanalysis data. NCDC, which damps its anomalies in data-sparse regions, shows the smallest anomaly amplitude. HadCRUT3 has the most missing data, but at where it does have data coverage, its amplitudes are quite similar to the other datasets. The results for the two geographically complete datasets, NCEP and ERA-40, are strikingly similar in the latitude and longitude locations of warming and cooling. The zonal-mean latitudinal profiles for the two reanalysis results are very close to each other, including even the Antarctic, except the rather larger cooling in Siberia seen in ERA-40 than in NCEP. GISS data is more similar to NCEP than ERA-40 in the Arctic region, with no zonally averaged cooling near 70° N. NCDC also does not show the severity of cooling in Siberia. We therefore find no support in the *in situ* data for the zonally averaged cooling found in the ERA-40 data in the Arctic.

The CMD Projection method [*Camp and Tung*, 2007] can be used to project the surface temperature from each of the dataset onto its own spatial pattern as determined by CMD. This results in a time series, which we then correlate with the solar TSI index to yield a correlation coefficient ρ. We test the statistical significance of this observed ρ for each dataset by generating 10,000 synthetic data using random assignment of years to solar groups, while preserving the same numbers of years in each group as in the observed case. Two confidence levels (in %) are listed in the figures. The first is obtained by counting the ratio of the realizations when $|\rho|$ >the observed value, and the second when $\rho >$ the observed value. By the first, more conservative, test, none of the *in situ* data reach statistical significance when projected onto the zonal mean CMD pattern, because of the missing data. However, since there is physical reason to believe that solar max warms [*Tung and Camp*, 2008], the second test is also a valid one, and by that test all datasets yield close to statistically significant positive correlations. The two reanalysis results are highly significant, as previously reported [*Camp and Tung*, 2007].

Next, we assume that the correct zonal-mean latitudinal structure for the solar cycle response should be given by that of NCEP, discussed above. We then proceed to project all five datasets onto the same geographically complete pattern determined by NCEP, normalized to have a global average of 1. The global mean surface temperature time series are shown in Figure 3. By filling in the area with missing data, this procedure yields a slightly larger global mean solar signal for the *in situ* dataset. A conservative measure of the amplitude of the response is given by κ, which is the regression coefficient of the projected time series shown in Figure 3 against the TSI time series, also shown. Discarding NCDC, whose interpolation scheme is not suitable for our study of anomaly signal, we see that *in situ* data yield a solar cycle signal of κ~0.12 K per 1 Wm^{-2} variation of solar constant. The amplitude of the solar cycle signal is larger in the reanalysis, as expected. NCEP is 0.19 K, and ERA-40 is 0.14 K. Note that these are not the peak-to-peak amplitudes, which are slightly over 0.2 K for both reanalysis dataset, and slightly less than 0.2 K for the GISS dataset. In subsequent sections we will adopt the range

$$\kappa \sim 0.12 - 0.19 \text{ K} /(\text{Wm}^{-2}). \quad (1)$$

The 2σ regression errors, indicated in the range of κ in Figure 3, are related to the goodness of fit of temperature response with TSI, and are affected by trend removal and method of analysis. These errors can be cut in half by using the LDA method [*Tung and Camp*, 2008], to 0.03-0.04 K/Wm^{-2}, smaller than the differences of the mean values between datasets indicated above, and will not be discussed further here.

HadCRUT3 data, when projected instead onto its 2D CMD pattern (see Figure 1), shows a statistically significant solar cycle signal despite its missing large amounts of data over continents. This appears to be due mostly to the solar cycle signal in the SST data over oceans, and the magnitude of the solar cycle signal, $\kappa \sim 0.1$ K per Wm^{-2}, is about the same as that found for sea-surface temperature [*White, et al.*, 1997].

4. Climate sensitivity parameter.

A measure of climate sensitivity can be defined as the ratio of the global-temperature response to the radiative forcing change,

$$\lambda=\delta T/(\varepsilon\delta F), \qquad (2)$$

where δF is the radiative forcing (RF) change for the troposphere, evaluated above the top of the troposphere. This quantity λ, called the climate sensitivity parameter, is expected to be different for different time scales. In order that the definition of the climate sensitivity parameter be more general, and applicable to the greenhouse forcing as well as solar-cycle forcing, the RF change in Eq. (2) is multiplied by the *efficac*y factor ε, which measures the ratio of a unit of RF of say the solar-cycle phenomenon to a unit of RF of CO_2 in terms of their effect in causing global warming, with the efficacy of the latter defined as identically 1. The models in AR4 have calculated values of efficacy for solar forcing close to 1, and all models in AR4 fall within the range of 0.7 to 1.0. Thus for solar-cycle forcing and response, we have

$$\lambda_{solar\text{-}cycle} = \delta T/(\varepsilon \delta F) \geq \delta T/(\delta F). \quad (3)$$

Eq (1) yields $\delta T/(\delta S)$. Using $\delta F_{solar\ cycle} = \delta S(1-\alpha)/4$, where the factor of four accounts for the geometry of the circular disk on which the solar constant is measured and the spherical area on which the RF is expressed and $\alpha \approx 0.3$ is the albedo, the fraction of the radiation reflected back to space by the surface and the clouds, Eq. (3) becomes

$$\lambda_{solar\ cycle} \geq 0.68 \text{ to} 1.08\ \mathrm{K/(Wm^{-2})}\ . \quad (4)$$

The definition of RF used by IPCC differs from the usual top of atmosphere value in that the former is evaluated at the top of the tropopause after the stratosphere has adjusted. Absorption of UV radiation by stratospheric ozone reduces the RF reaching the tropopause from the top of the atmosphere. Since 12-15% of the solar variability lies in the UV range (below 295 nm)[*Lean, et al.*, 1997], this reduction can potentially be as large as 12-15%. The stratospheric adjustment involves both the warmer temperature by the enhanced UV heating, which increases the longwave radiation reaching the troposphere, and the enhanced production of stratospheric ozone. More ozone not only reduces further the shortwave radiation to the troposphere not absorbed by the existing ozone, but enhances the downward longwave radiation. There is some uncertainty in the net change in RF caused by the different predicted vertical distribution of enhanced ozone, as reviewed in Table 4.1 of *Gray et al.* [2005]. We take the result from *Larkin, et al.* [2000], RF~0.18 $\mathrm{Wm^{-2}}$, which happens to be the same as the top of atmosphere estimate. This is also consistent with Chapter 2 of the latest IPCC report [*Forster, et al.*, 2007], where the RF of the 11-year solar-cycle variability is not reduced by the stratospheric absorption, citing compensation by indirect effect of solar-ozone interaction in the stratosphere (see footnote 11 therein). This solar RF turns out to be almost 1/20 that for the total change in RF due to a doubling of CO_2 ($RF \approx 3.7$ Wm^{-2}). Therefore the annual rate of increase in radiative forcing of the lower atmosphere during the five years from solar min to solar max happens to be equivalent to that from an average simple 1% per year increase in greenhouse gases. The global pattern of warming and cooling for the solar cycle signal shown in Figure 1 is also quite similar to the IPCC AR4 global warming runs as shown in [*Leroy, et al.*, 2006].

A climate sensitivity parameter for model TCR can be defined as

$$\lambda_{TCR}=\delta T/\delta F=TCR/3.7 \text{ Wm}^{-2}. \quad (5)$$

Since TCR is defined as the δT at the time of doubled CO_2 after it has been increasing at a *compounded* rate of 1% per year, the instantaneous change in RF responsible for TCR is larger than the average annual rate, and so we expect the response, which is the TCR, to be larger than the average δT. Thus

$$\lambda_{TCR} > \lambda_{solar\ cycle} \geq 0.68 \text{ to} 1.08 \text{ K/(Wm}^{-2}). \quad (6)$$

By multiplying Eq. (6) by $\delta F=3.7$ Wm^{-2} we obtain the desired constraint:

$$TCR > 2.5 \text{ to } 4.0 \text{ K}. \quad (7)$$

The equilibrium climate sensitivity (ECS) should be greater than TCR, constrained by (7).

The difference in the time scales between an oscillatory forcing and a secular forcing works in the direction of the inequality in (7). For the TCR, at the time of evaluation, there have been 70 years of compound 1% increase in RF, and the delayed heating due to ocean inertia adds to the instantaneous heating, while for the solar-cycle response at solar max, there have only been only five heating years.

The TCRs of 19 coupled atmosphere-ocean GCMs in IPCC AR4 listed in Table 1 fall within the rather low range of 1.2-2.2 K with the exception of one, and thus *fail* the lower constraint of 2.5 K determined by the interpolated *in situ* data of GISS and HadCRUT3. The only exception is the Japanese MIROC (hi-res), with a TCR of 2.6 K. All models fail the higher constraint of 4.0 K determined by the NCEP data.

5. Conclusion

We have examined five datasets on global surface temperature, two reanalyses and three *in situ*. We can establish the existence of a solar cycle signal in all five datasets at a confidence level above 95%. The magnitude of the signal is less in the *in situ* data than in the reanalysis data, due to the missing data coverage. Nevertheless, the peak-to-peak amplitude in the *in situ* data is only slightly less than the 0.2 K of the two reanalysis datasets. The measured solar response is then used to provide a constraint on the transient climate response of models.

It is seen that most of the current generation of general circulation models assessed by IPCC, AR4, are found to have too low a transient climate response as compared with the observed transient climate sensitivity obtained by our method. This is consistent with the independent finding by *Forest et al.* [2006] that models simulate too large an ocean heat uptake as compared to observations of ocean temperature changes during the period 1961-2003. This excessive heat into the oceans tends to reduce the transient climate response for the atmosphere, but does not affect the modeled equilibrium climate sensitivity, which was calculated with a slab ocean in thermal equilibrium with the atmosphere.

Acknowledgements.The research is supported by grant ATM-03 32364 from National Science Foundation, Climate Dynamics Program. We thank Professor Brian Farrell for encouraging us to investigate the climate sensitivity implications of our solar-cycle work.

References

Brohan, P., J. J. Kennedy, I. Harris, S. F. B. Trett, and P. D. Jones (2006), Uncertainty estimates in regional and global observed temperature changes: a new data set from 1850, *J. Geophys. Res.*, *111*, doi:10.1029/2005JD006548.

Camp, C. D., and K. K. Tung (2007), Surface warming by the solar cycle as revealed by the composite mean difference projection, *Geophysical Research Letters*, *34*, L14703, doi:14710.11029/12007GL030207.

Forest, D. J., P. Stone, and A. P. Sokolov (2006), Estimated PDFs of climate system properties including natural and anthropogenic forcings, *Geophys. Research. Lett.*, *33*, doi:10.1029/2005GL023977.

Forster, P. M., V. Ramaswamy, P. Artaxo, and E. al. (2007), Changes in atmospheric constituents and in radiative forcing. In: Climate Change 2007: The Physical Science Basis., in *Contribution of Working Group I to the Fourth Assessment Report of the Intergovernmental Panel on Climate Change.*, edited by S. Solomon, D. Qin, M. Manning, Z. Chen, M. Marquis, K. B. Averyt, M. Tignor and H. L. Miller, pp. 129-234, Cambridge University Press, Cambridge, United Kingdom and New York, USA.

Gray, L. J., J. D. Haigh, and R. G. Harrison (2005), A Review of the influence of solar changes on the Earth's climate, *Hadley Center Technical Note 62*, 82 pages.

Hansen, J., R. Ruedy, J. Glascoe, and M. Sato (1999), GISS analysis of surface temperature change, *J. Geophys. Res.*, *104*, 30,997-931,022.

Hansen, J., G. L. Russell, A. Lacis, I. Fung, and D. Rind (1985), Climate response times: Dependence on climate sensitivity and ocean mixing, *Science*, *229*, 857-859.

Kalnay, E., M. Kanamitsu, R. Kistler, W. Collins, D. Deaven, L. Gandin, M. Iredell, S. Saha, G. White, J. Woollen, Y. Zhu, M. Chelliah, W. Ebisuzaki, W. Higgins, J. Janowiak, K. C. Mo, C. Ropelewski, J. Wang, A. Leetmaa, R. Reynolds, R. Jenne, and D. Joseph (1996), The NCEP/NCAR 40-year reanalysis project, *Bull. Amer. Meteorol. Soc.*, *77*, 437-471.

Larkin, A., J. D. Haigh, and S. Djavidnia (2000), The effect of solar UV irradiance variations on the Earth's atmosphere, *Space Sci. Rev.*, *94*, 199-214.

Lean, J. L., G. J. Rottman, H. L. Kyle, T. N. Woods, J. R. Hickey, and L. C. Puga (1997), Detection and parameterization of variations in solar mid- and near-ultraviolet radiation (200-400 nm), *J. Geophys. Res.-Atmos.*, *102*, 29939-29956.

Leroy, S. S., J. G. Anderson, and J. A. Dykema (2006), Testing climate models using GPS radio occultation: A sensitivity analysis, *J. Geophys. Res.*, *111*, doi:10.1029/2005JD006145.

Marshall, J., D. Ferreira, J. M. Campin, and D. Enderton (2007), Mean climate and variability of the atmosphere and ocean on an aquaplanet., *J. Atmos. Sci.*, *64*, 4270-4286.

Peterson, T. C., and R. S. Vose (1997), An overview of the Global Historical Climatological Network temperature database, *Bull. Amer. Meteorol. Soc.*, *78*, 2837-2849.

Randall, D., R. Wood, S. Bony, R. Colman, T. Fichefet, J. Fyfe, V. M. Kattsov, A. Pitman, J. Shukila, J. Srinivasan, R. J. Stouffer, A. Sumi, and K. E. Taylor (2007), Climate models and their evaluation. In: Climate Change 2007: The Physical Science

Basis., in *Contribution of Working Group I to the Fourth Assessment Report of the Intergovernmental Panel on Climate change*, edited by A. Solomon, D. Qin, M. Manning, Z. Chen, M. Marquis, K. B. Averyt, M. Tignor and H. L. Miller, Cambridge University Press, Cambridge, United Kingdom and New York, NY, USA.

Rayner, N. A., P. Brohan, D. E. Parker, C. K. Folland, J. J. Kennedy, M. Vanicek, T. J. Ansell, and S. F. B. Trett (2006), Improved analyses of changes and uncertainties in sea-surface temperature measured in-situ since the mid-nineteenth century, *J. Climate.*, *19*, 446-469.

Reynolds, R. W., and T. M. Smith (1994), Improved global sea surface temperature analyses, *J. Climate.*, *7*, 929-948.

Seager, R., N. Harnik, and Y. Kushnir (2003), Mechanisms of hemispherically symmetric climate variability, *J. Climate.*, *16*, 2960-2978.

Smith, T. M., and R. Reynolds (2005), a global merged land-air-sea surfact temperature reconstruction based on historical observations (1880-1997), *J. Climate.*, *18*, 2021-2036.

Smith, T. M., R. W. Reynolds, R. E. Livesay, and D. C. Stokes (1996), Reconstruction of historical sea surface temperature using empirical orthogonal functions, *J. Climate.*, *9*, 1403-1420.

Stott, P. A., and e. al. (2006), Observational constraints on past attributable warming and predictions of future global warming, *J. Climate.*, *19*, 3055-3069.

Tung, K. K., and C. D. Camp (2008), Solar-cycle warming of the earth's surface in NCEP and ERA-40 data, a Linear Discriminant Analysis, *J. Geophys. Res.*, *113*, D05114, doi:05110.01029/02007JD009164.

Uppala, S. M., P. W. Kallberg, A. J. Simmons, U. Andrae, V. D. Bechtold, M. Fiorino, J. K. Gibson, J. Haseler, A. Hernandez, G. A. Kelly, X. Li, K. Onogi, S. Saarinen, N. Sokka, R. P. Allan, E. Andersson, K. Arpe, M. A. Balmaseda, A. C. M. Beljaars, L. Van De Berg, J. Bidlot, N. Bormann, S. Caires, F. Chevallier, A. Dethof, M. Dragosavac, M. Fisher, M. Fuentes, S. Hagemann, E. Holm, B. J. Hoskins, L. Isaksen, P. A. E. M. Janssen, R. Jenne, A. P. McNally, J. F. Mahfouf, J. J. Morcrette, N. A. Rayner, R. W. Saunders, P. Simon, A. Sterl, K. E. Trenberth, A. Untch, D. Vasiljevic, P. Viterbo, and J. Woollen (2005), The ERA-40 re-analysis.

White, W. B., J. Lean, D. R. Cayan, and M. D. Dettinger (1997), Response of global upper ocean temperature to changing solar irradiance, *J. Geophys. Res.-Oceans*, *102*, 3255-3266.

AOGCM	Equilibrium climate sensitivity (°C)	Transient climate response (°C)
1: BCC-CM1	n.a.	n.a.
2: BCCR-BCM2.0	n.a.	n.a.
3: CCSM3	2.7	1.5
4: CGCM3.1(T47)	3.4	*1.9*
5: CGCM3.1(T63)	*3.4*	n.a.
6: CNRM-CM3	n.a.	1.6
7: CSIRO-MK3.0	3.1	1.4
8: ECHAM5/MPI-OM	3.4	2.2
9: ECHO-G	3.2	1.7
10: FGOALS-g1.0	*2.3*	*1.2*
11: GFDL-CM2.0	2.9	1.6
12: GFDL-CM2.1	3.4	1.5
13: GISS-AOM	n.a.	n.a.
14: GISS-EH	2.7	1.6
15: GISS-ER	2.7	1.5
16: INM-CM3.0	2.1	1.6
17: IPSL-CM4	4.4	2.1
18: MIROC3.2(hires)	4.3	2.6
19: MIROC3.2(medres)	4.0	2.1
20: MRI-CGCM2.3.2	3.2	2.2
21: PCM	2.1	1.3
22: UKMO-HadCM3	3.3	2.0
23: UKMO-HadGEM1	4.4	1.9

Table 1. Equilibrium Climate Sensitivity and Transient Climate Response for various Atmosphere-Ocean GCMs assessed by IPCC AR4.

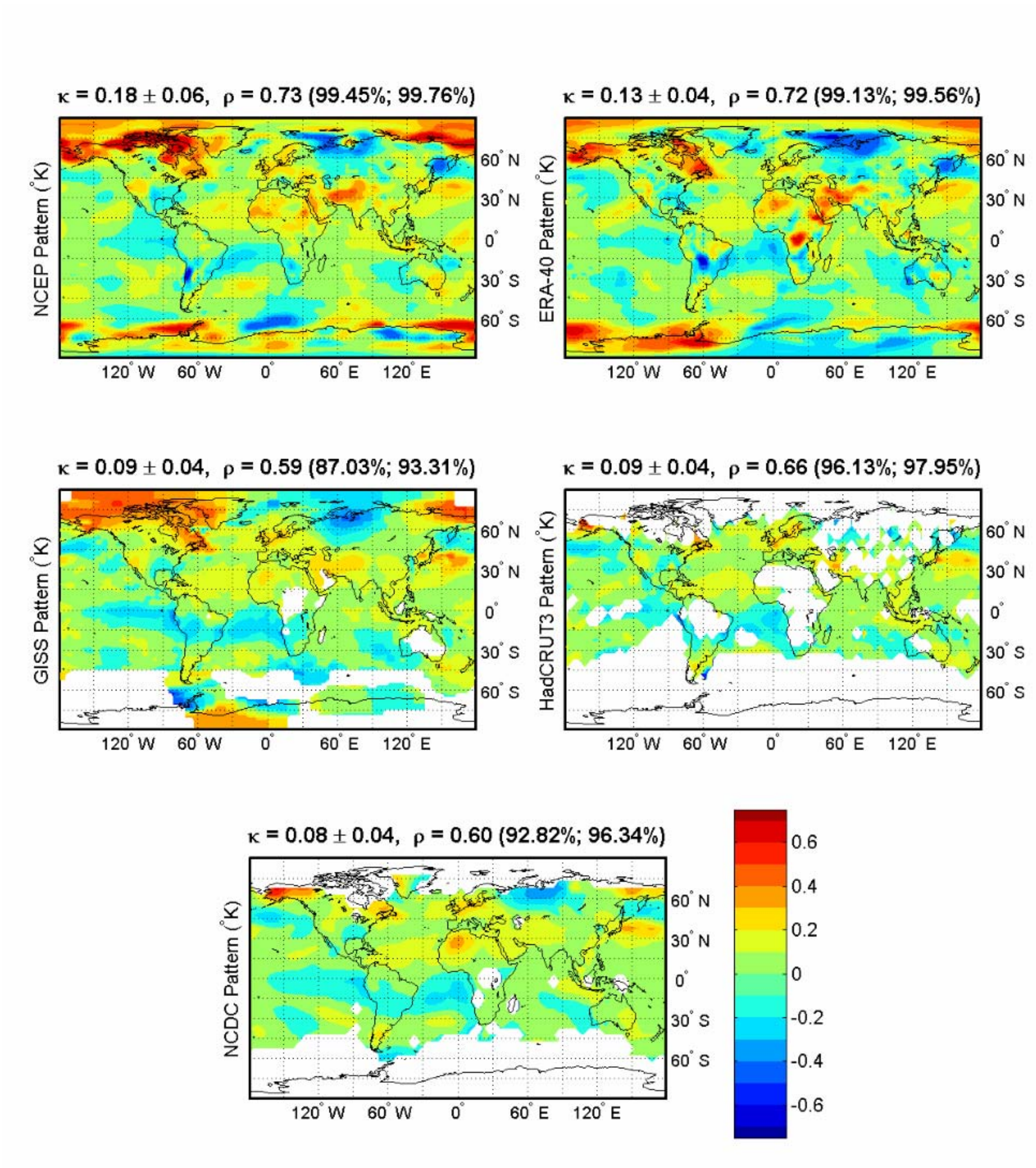

Figure 1. Composite mean difference between solar max-min years in surface temperature in K; missing data areas are left blank, except for HadCRUT3, where the composites are calculated with 5/6 of data available at that location. Annual average is the average of seasons, provided that at least three seasons are available and the missing season is not winter or summer. Seasonal average is the average of three months in the season, provided that at least two months are available.

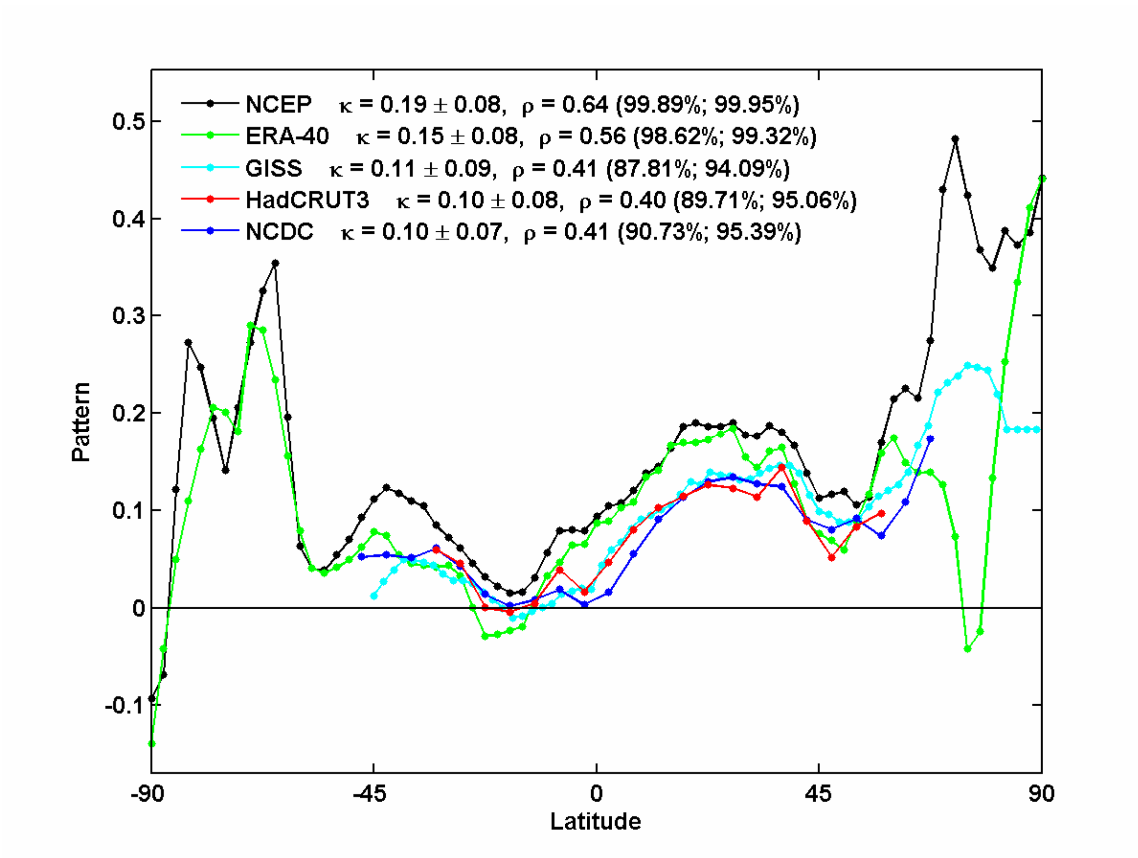

Figure 2. Zonal mean composite mean difference between solar max years and solar min years. Zonal means are taken if 2/3 of the data are available on a zonal circle.

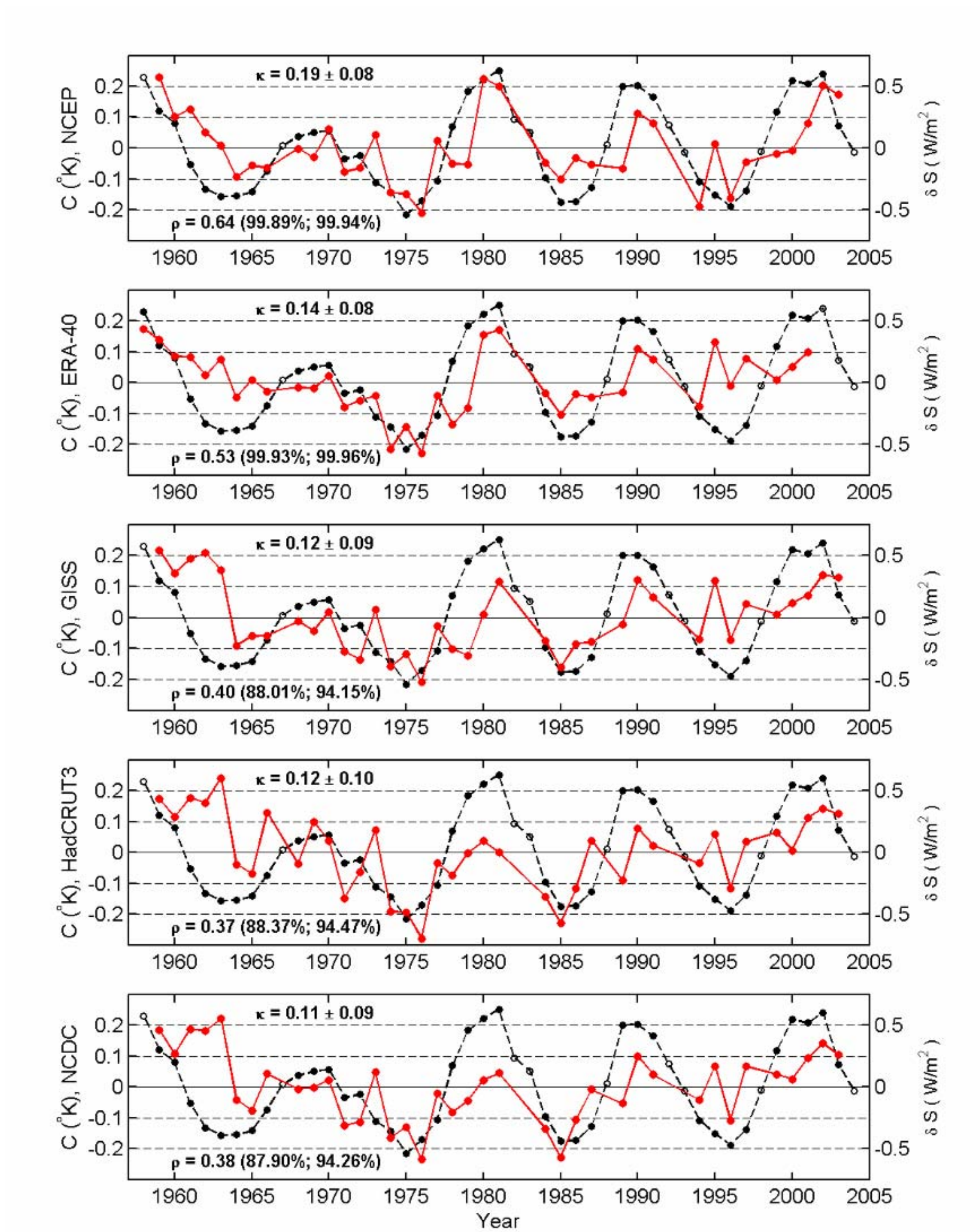

Figure 3. Surface temperature CMD Projection of each of the five datasets onto the zonal mean spatial pattern determined by the geographically complete NCEP reanalysis, normalized in such a way that the left axis indicates the globally averaged value. The dotted line is the TSI index, whose scale is shown on the right axis.